J. Fluid Mech. (1988), *vol.* 193, *pp.* 347–367
Printed in Great Britain

The effect of secondary motion on axial transport in oscillatory tube flow

By T. J. PEDLEY† AND R. D. KAMM‡

† Department of Applied Mathematics and Theoretical Physics, University of Cambridge, Silver Street, Cambridge CB3 9EW, UK

‡ Department of Mechanical Engineering, Massachusetts Institute of Technology, Cambridge, MA 02139, USA

(Received 25 May 1987 and in revised form 7 March 1988)

In oscillatory flows through systems of branched or curved tubes, Taylor dispersion is modified both by the oscillation and by the induced secondary motions. As a model for this process, we examine axial transport in an annular region containing an oscillatory axial and steady secondary (circumferential) flow. Two complementary approaches are used: an asymptotic analysis for an annulus with a narrow gap (δ) and for large values of the secondary flow Péclet number (P); and a numerical solution for arbitrary values of δ and P. The results exhibit a form of resonance when the secondary-flow time equals the oscillation period, giving rise to a prominent maximum in the transport rate. This observation is consistent with preliminary numerical results for oscillatory flow in a curved tube, and can be explained physically.

1. Introduction

Taylor (1953) first analysed the mixing of a bolus of marked fluid in steady laminar and turbulent flow in long straight tubes, far from the ends and from the site at which the bolus was introduced. In those cases he showed that the longitudinal spreading could be described as a diffusive process, with an effective diffusivity proportional to the square of a typical axial velocity difference between different fluid elements, multiplied by the timescale for an individual solute molecule to sample all cross-stream locations at which different velocities exist. The more vigorous the mass transfer laterally (by diffusion, turbulence, etc.), the more restricted is the axial dispersion of the bolus. Subsequent workers have analysed the corresponding process for time-dependent laminar flow in a straight tube (Chatwin 1975; Watson 1983), and the results have been successfully tested experimentally (Joshi *et al.* 1983). In many applications, however, the tubes are curved or branched, resulting in vigorous secondary motions which are likely to be the dominant source of the lateral mixing involved in Taylor dispersion. One such application of particular interest involves the transport of gas through the airways of the lung during artificial ventilation with small-volume, high-frequency oscillation (Drazen, Kamm & Slutsky 1984). Others include dispersion in rivers or estuaries or in piping systems which typically involve bends and branching.

Despite its importance, there has been relatively little work on the effects of secondary motions on Taylor dispersion. Erdogan & Chatwin (1967) and Nunge, Lin & Gill (1972) studied the problem of longitudinal dispersion in steady curved-tube

flow by asymptotic expansions, and found that the effect of secondary motion becomes important when Dn^2Sc exceeds about 10^2, where

$$Dn = \frac{aw_0}{\nu}\left(\frac{a}{R}\right)^{\frac{1}{2}} \tag{1.1}$$

is the Dean number, assumed small by those authors, and

$$Sc = \nu/\kappa \tag{1.2}$$

is the Schmidt number. Here a is the radius and R the radius of curvature of the tube, w_0 is the mean axial velocity, and ν, κ are the kinematic viscosity and solute or gas diffusivity of the fluid. The quantity Dn^2Sc is a secondary-flow Péclet number

$$P = V_s a/\kappa, \tag{1.3}$$

since the scale V_s for secondary-flow velocities is $Dn^2\nu/a$ when Dn is small (Dean 1928).

These results have been extended numerically by Janssen (1976) and by Johnson & Kamm (1986). Both studies show a fall in the effective diffusivity due to the mixing associated with secondary flow, until at large values of Dn^2Sc mixing along the secondary-flow streamlines is complete and isoconcentration contours generally line up with the secondary-flow streamlines. This occurs for $Dn^2Sc > 10^5$, when mixing *along* secondary-flow streamlines, as augmented by shear dispersion of the type described by Rhines & Young (1983) (see below), occurs on a timescale small compared with that for mixing *between* streamlines by molecular diffusion.

The same techniques as those of Johnson & Kamm (1986) have been used to study the combined effects of oscillatory flow of period T, and curvature (Sharp 1987). He considered oscillatory, quasi-steady, fully developed flow in a curved tube and computed the convective and diffusive motions of a cloud of solute molecules for sufficiently high Sc that the concentration distribution was not quasi-steady. The axial variance of this cloud is used to calculate an effective diffusivity following the method of Johnson & Kamm (1986). The results (figure 1) showed that for $Dn^2Sc > 100$ and

$$\beta^2 (= 2\pi a^2/\kappa T) > 1, \tag{1.4}$$

the region not previously studied, there appeared to be a maximal transport rate associated with the condition $Dn^2Sc/\beta^2 \approx$ const. In other words, a maximum is observed when the secondary-flow time is of the same order as the cycle period. Figure 1 also indicates that the peak effective diffusivity diminishes somewhat as Dn^2Sc increases and it is therefore of interest to investigate the limit of large secondary-flow Péclet number.

In this paper we investigate the effect of an interaction between secondary flows and oscillations on longitudinal mixing by way of a simple model. Consider, for example, the annular region bounded by any pair of secondary streamlines in the cross-sectional plane of a curved tube as sketched in figure 2 (*a*). Within this distorted annulus, fluid particles experience oscillations in axial velocity due to their advection around the annulus and to the time-periodic axial flow. Fluid particles in the imaginary annulus periodically experience axial velocities both greater than (+) and less than (−) the mean axial velocity on a particular streamline. Furthermore, if we restrict attention to flows for which the frequency parameter α, defined by

$$\alpha^2 = \beta^2/Sc = 2\pi a^2/\nu T, \tag{1.5}$$

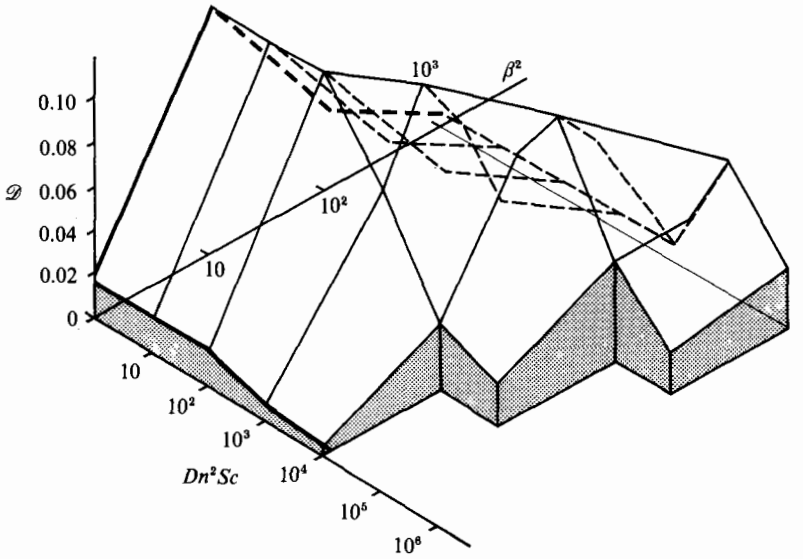

FIGURE 1. Results of a Monte Carlo simulation for normalized axial transport coefficient $\mathscr{D} = D_{\text{eff}}/w_0^2 T$ as a function of β^2 and Dn^2Sc (Sharp 1987).

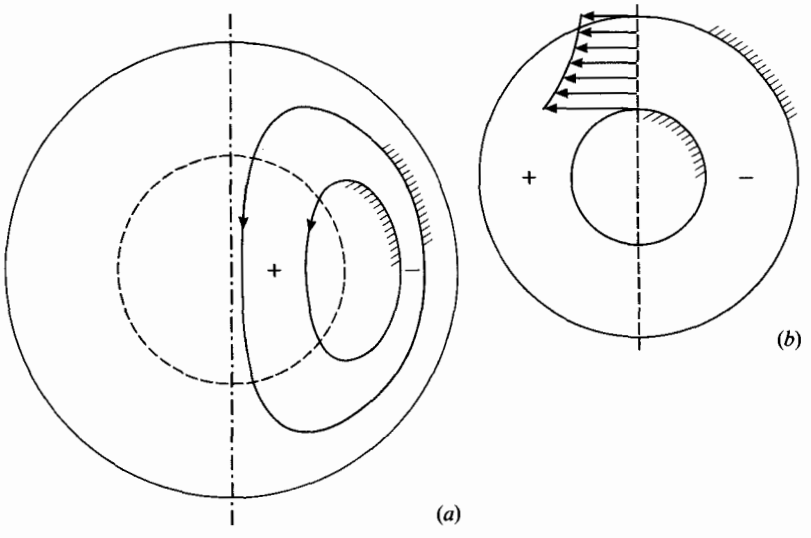

FIGURE 2. (*a*) Secondary streamlines for flow in a curved tube, with simultaneous axial oscillation; + and − represent regions in which the axial velocity has opposite signs (relative to the mean) at any instant. Hatchings represent the boundaries of an annular region, in which the flow is analogous to that in the annulus investigated in this paper and depicted in (*b*).

is small and Dn not too large, the axial and secondary velocities are quasi-steady and the streamline pattern is time-independent. In the model problem (figure 2*b*) the fluid is contained in a circular annulus and experiences an oscillatory axial flow which, at any instant, has opposite signs on opposite sides of the annulus, together with a steady circumferential (secondary) flow. The model thus contains most of the important features of curved-tube flow. While somewhat idealized, the justification for the model lies primarily in the fact that it leads to a tractable mathematical

problem and hence to physical insight. Those aspects of the curved-tube problem that are not contained in the model problem are discussed in §6.

Before giving a mathematical formulation and solution of the model problem, in the next section we present physical arguments leading to dimensional scaling laws for the effective diffusivity in various parameter ranges.

2. Dimensional scaling

Consider, first, purely oscillatory flow in an infinitely long straight tube and let the instantaneous axial velocity of a particle relative to the mean velocity w_0 be $w_{\rm rel} = w - w_0$. The relative convective flux of some species across a cross-section A normal to the axis is

$$\hat{F} = \overline{\frac{1}{A}\int_A w_{\rm rel}\,\theta\,\mathrm{d}A}, \tag{2.1}$$

where θ is species concentration and the overbar denotes a time average. The effective axial diffusivity, $D_{\rm eff}$, is defined by

$$\hat{F} = -D_{\rm eff}\frac{\mathrm{d}}{\mathrm{d}z}\left(\frac{1}{A}\int_A \bar{\theta}\,\mathrm{d}A\right), \tag{2.2}$$

where z is the axial coordinate. Now, if $w_{\rm rel}(t)$ is a stationary random process, we can write

$$D_{\rm eff} = \frac{1}{A}\int_A \mathrm{d}A \int_0^\infty \langle w_{\rm rel}(t)\, w_{\rm rel}(t-t')\rangle\,\mathrm{d}t', \tag{2.3}$$

where $\langle\ \rangle$ denotes an ensemble average which is independent of t for large t (Taylor 1921). Equation (2.3) suggests the following scaling for $D_{\rm eff}$:

$$D_{\rm eff} \sim w_{\rm rel}^2\, t_{\rm c}\, \mathscr{A}, \tag{2.4}$$

where $t_{\rm c}$ is the time during which the relative velocity of a particle remains correlated with its initial value, $w_{\rm rel}$ is a characteristic value of relative axial velocity sampled in time $t_{\rm c}$, and $\mathscr{A}$ is the fraction of A occupied by the velocity differences. Thus, for steady flow in a straight pipe (Taylor 1953), $t_{\rm c}$ equals the lateral diffusion time $t_{\rm d}(\sim a^2/\kappa)$, $w_{\rm rel} \approx w_0$ and $\mathscr{A} = 1$, giving the familiar result

$$D_{\rm eff} \sim w_0^2 a^2/\kappa. \tag{2.5}$$

In oscillatory flow with period T, the velocity and concentration distributions are quasi-steady if $t_{\rm d}/T \ll 1$, provided $Sc = \nu/\kappa \geqslant 1$, and then the above result applies. This can be normalized to read

$$\mathscr{D} = \frac{D_{\rm eff}}{w_0^2 T} \sim \frac{t_{\rm d}}{T}\,(= \beta^2) \quad \text{for} \quad \frac{t_{\rm d}}{T} \ll 1. \tag{2.6}$$

If, on the other hand, $t_{\rm d}/T \gg 1$ and $Sc \gg 1$, so that $\alpha^2 \ll 1$, then although the flow is quasi-steady, the concentration distribution, and hence the mass transfer, is not. The axial displacement of a fluid particle relative to the mean results from its lateral diffusion in the shear flow, which is uncorrelated in successive half-periods, giving $t_{\rm c} \sim T$. Since the shear is still distributed over the entire cross-section, $\mathscr{A} = 1$ and $w_{\rm rel} \sim (\mathrm{d}w/\mathrm{d}r)\,\delta_{\rm c}$ where $\delta_{\rm c}$ is the distance of lateral diffusion in time $t_{\rm c}$: $\delta_{\rm c} \sim (\kappa T)^{\frac{1}{2}}$. Combining, we obtain

$$\mathscr{D} \sim \frac{T}{t_{\rm d}} \quad \text{for} \quad \frac{t_{\rm d}}{T} \gg 1, \quad Sc \gg 1. \tag{2.7}$$

If, on the other hand, $t_d/T \gg 1$ and $\alpha^2 \gg 1$ (so Sc is not necessarily $\gg 1$), the velocity and concentration distributions are both unsteady and velocity gradients are confined to a narrow boundary layer near the wall of thickness $\delta_v \sim (\nu T)^{\frac{1}{2}}$. In this case, $t_c \sim T$, $\mathscr{A} \sim \delta_v/a$ and $w_{rel} \sim w_0 \delta_c/\delta_v \sim w_0(\kappa/\nu)^{\frac{1}{2}}$. Hence

$$\mathscr{D} \sim \left(\frac{T}{t_d}\right)^{\frac{1}{2}} \frac{1}{Sc^{\frac{1}{2}}} \quad \text{for } \frac{t_d}{T} \gg 1, \quad Sc \sim O(1). \tag{2.8}$$

These results, which are consistent with previous analytical (Chatwin 1975; Watson 1983) and experimental (Joshi *et al.* 1983) studies, give rise to the maximum in $\mathscr{D}$ seen in figure 1 for $t_d/T \sim O(1)$.

A similar approach can be used in the presence of secondary motions. Consider oscillatory flow in a tube with secondary motions characterized by a velocity scale V_s and a circulation time, $t_s \sim a/V_s$. Now t_d/t_s is the secondary-flow Péclet number (1.3). If this is small, the secondary motions have little effect on lateral mixing and the results given above for a straight tube ((2.5)–(2.8)) apply. If $t_d/t_s \gg 1$ but $t_d/T \ll 1$, the flow is quasi-steady but secondary motions are important. As shown by Johnson & Kamm (1986), the effect of secondary flow is to distort the θ-distribution from a radially symmetric pattern (where $t_d/t_s \ll 1$) to one in which the isoconcentration contours line up with the secondary-flow streamlines (for $t_d/t_s \gg 1$). In both limits the lateral mixing time is established by molecular diffusion and a result similar to (2.6) is obtained:

$$\mathscr{D} \sim \frac{t_d}{T} f\left(\frac{t_d}{t_s}\right), \tag{2.9}$$

where $f(t_d/t_s)$ is a weak function, ranging between 1.0 and 0.2 as t_d/t_s ranges from about 1 to 10^3.

When $t_d/t_s \gg 1$ and $t_d/T \gg 1$, both unsteadiness and curvature are likely to be important. Here we have only the preliminary numerical results of figure 1 to guide us, indicating a maximum in transport rate when $t_s/T = O(1)$. This condition corresponds to a sort of *resonance* in that the axial velocity at a point changes direction twice in the time it takes a particle to complete a circuit around the secondary-flow streamline. Consider a fluid particle on a particular secondary-flow streamline, for which the circulation time is exactly T, and suppose that w_{rel} for this particle is positive when the bulk velocity is also positive. Then, at resonance, w_{rel} will still be positive when the bulk flow velocity is negative; the particle's velocity will have been rectified, and the axial motion of a fluid particle can remain correlated with its initial value over many cycles. In fact, it remains correlated until such time that the particle migrates around the streamline (or away from it) by some diffusive process.

The process for mixing along a closed streamline was analysed for large values of P by Rhines & Young (1983). They showed that homogenization of the concentration distribution (or 'expulsion of concentration gradients') takes place in two stages, rapid and slow. The rapid stage consists of the transformation of an arbitrary initial distribution into one that is uniform along individual streamlines but varies from one to another, while the slow stage consists of a gradual diffusive smoothing between streamlines (timescale t_d). The timescale for the rapid stage is governed by shear dispersion in the secondary flow, and is given by

$$t_a \sim a^{\frac{4}{3}}/\kappa^{\frac{1}{3}} V_s^{\frac{2}{3}} \sim t_d P^{-\frac{2}{3}}. \tag{2.10}$$

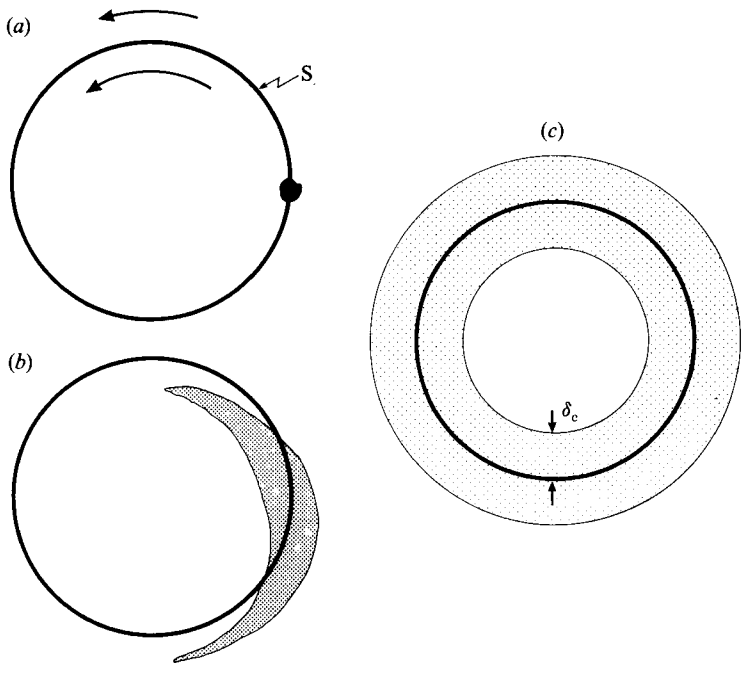

FIGURE 3. Sketch showing how a solute blob placed at one location on the streamline S (*a*) simultaneously diffuses to neighbouring streamlines and is stretched due to secondary shear (*b*), ultimately becoming uniformly mixed around the entire circumference (*c*).

To understand this result, consider a blob of high concentration centred on one streamline S (figure 3). Solute diffuses to neighbouring streamlines where, as a result of secondary shear, the velocity is different, causing the blob to be stretched in the streamwise direction. Diffusion back to S then smoothes out the initial non-uniform concentration along S. The time t_a is the time required for the outer part of the spreading blob, a transverse distance δ_c from S, say, to travel a distance $O(a)$ relative to a particle on S. That is,

$$t_a = \frac{a}{\Delta V} = \frac{\delta_c^2}{\kappa}, \tag{2.11}$$

where ΔV is the difference in velocity on streamlines a distance δ_c apart. If, as in a curved tube, the local velocity gradient can be scaled by V_s/a, then $\Delta V \sim V_s \delta_c/a$ and (2.11) gives

$$\delta_c = (\kappa a^2/V_s)^{\frac{1}{3}}, \tag{2.12}$$

the familiar scale for (quasi-) steady concentration boundary-layer thickness in a shear flow (Lévêque 1928) and (2.10) follows. We may note in addition that t_a can also be evaluated as a 'secondary Taylor dispersion' time, a^2/D_{SE}, where $D_{SE} = \Delta V^2 \delta_c^2/\kappa$ is the scale for the effective diffusivity for shear dispersion *along* the secondary streamlines, as given by a formula like (2.5).

We can now envisage a region of width δ_c surrounding that streamline for which exact resonance occurs ($t_s = T$), and within which particle axial velocities are correlated; we call this region the 'critical layer'. Using the general approach developed above, we have $w_{rel} \sim w_0$, $t_c \sim t_a$ and the area that takes part in this

transport process is $2\pi\delta_c a$, giving $\mathscr{A} \sim \delta_c/a$. Combining these scaling relations with (2.4) and (2.11) yields

$$\mathscr{D} \sim \frac{t_s}{T} \sim 1,$$

which accounts for the ridge of constant $\mathscr{D}$ found for $t_s/T = O(1)$ in figure 1. These scalings are confirmed by the analytical and numerical solutions that follow.

3. Formulation of the model problem

We consider the transport of solute in a uniform, effectively straight tube, with cross-section $\hat{A}$ of dimension a, containing an incompressible fluid. The flow is independent of axial coordinate $\hat{z}$ ($\hat{}$ denotes a dimensional variable) but has transverse as well as axial velocity components which scale with different velocities V_s and w_0 respectively and which are supposed known. We suppose, following previous authors such as Taylor (1953), that the solute concentration $\hat{\theta}$ is made up of a uniform axial gradient on which is superimposed a perturbation which depends only on transverse coordinates $(\hat{x}, \hat{y})$ and t. That is

$$\hat{\theta} = -\hat{G}\hat{z} + \hat{\theta}_0\,\theta(x, y, t), \tag{3.1}$$

where $(x, y) = (\hat{x}/a, \hat{y}/a)$ and $\hat{\theta}_0$ is a scale for the concentration fluctuations, chosen for convenience to be

$$\hat{\theta}_0 = \hat{G}aw_0/V_s.$$

If the velocity components are non-dimensionalized appropriately, i.e. we take $(u, v, w) = (\hat{u}/V_s, \hat{v}/V_s, \hat{w}/w_0)$, the convection–diffusion equation becomes

$$\frac{\partial\theta}{\partial t} + \boldsymbol{u}\cdot\boldsymbol{\nabla}\theta = w + \frac{1}{P}\nabla^2\theta, \tag{3.2}$$

where vectors and vector operators are two-dimensional, i.e. $\boldsymbol{u} = (u, v)$ and $\boldsymbol{\nabla} = (\partial/\partial x, \partial/\partial y)$, t is the time non-dimensionalized with respect to the secondary-flow circulation timescale a/V_s, and P is the secondary-flow Péclet number, given by (1.3). Equation (3.2) is to be solved subject to the boundary condition

$$\frac{\partial\theta}{\partial n} = 0 \tag{3.3}$$

on the cross-sectional boundary $\partial\hat{A}$, assumed smooth. The output of the calculation should be the mean axial solute flux, less that resulting directly from either molecular diffusion of the mean concentration gradient or advection of the mean gradient with the mean axial velocity if there is one. That is, we seek

$$\hat{F} = \frac{1}{\hat{A}}\left\langle \iint_A \hat{w}(\hat{\theta} + \hat{G}\hat{z})\,\mathrm{d}\hat{x}\,\mathrm{d}\hat{y} \right\rangle = \hat{G}a^2\frac{w_0^2 a}{V_s}F, \tag{3.4}$$

where $\langle\ \rangle$ represents a time mean, and

$$F = \frac{1}{A}\left\langle \iint_A w\theta\,\mathrm{d}x\,\mathrm{d}y \right\rangle \tag{3.5}$$

is the dimensionless additional flux. The effective longitudinal diffusivity is given by (2.2) to be

$$D_{\text{eff}} = \frac{w_0^2 a}{V_s} F, \tag{3.6}$$

and $A = \iint_A \mathrm{d}x\,\mathrm{d}y$ is the dimensionless cross-sectional area.

We now postulate that the axial flow is purely oscillatory with zero mean, i.e.

$$w = \mathrm{Re}\{W(\boldsymbol{r})\, \mathrm{e}^{\mathrm{i}\omega t}\},$$

where $\boldsymbol{r} = (x, y)$ and $\omega = 2\pi a/V_s T \propto t_s/T$ is the dimensionless frequency. Note that, in terms of the dimensionless effective diffusivity $\mathscr{D}$ introduced in §2, we have

$$\mathscr{D} = \frac{\omega F}{2\pi}. \tag{3.7}$$

The secondary velocity field $\boldsymbol{u}$ is taken to be steady (as discussed in §1) and we can therefore postulate a solution of (3.2) in which

$$\theta = \mathrm{Re}\{c(\boldsymbol{r})\, \mathrm{e}^{\mathrm{i}\omega t}\},$$

where c is a complex function. The equation for c is

$$\mathrm{i}\omega c + \boldsymbol{u}\cdot\nabla c = W + \frac{1}{P}\nabla^2 c, \tag{3.8}$$

with boundary condition $\partial c/\partial n = 0$ on ∂A, and the dimensionless mean excess flux is

$$F = \frac{1}{2A}\,\mathrm{Re}\left\{\iint_A W^* c\,\mathrm{d}x\,\mathrm{d}y\right\}, \tag{3.9}$$

where W^* is the complex conjugate of W.

In the next two sections we look at simple examples in which the secondary flow has circular streamlines, and we solve (3.8) using polar coordinates (r, ϕ), in an annular domain bounded by the impermeable boundaries $r = 1$ and $r = 1+\delta$. We choose secondary velocity fields from the family given by

$$u_r = 0, \quad u_\phi \equiv V(r) = Ar + \frac{B}{r} \tag{3.10}$$

for some constants A, B, in order that the (r, ϕ)-components of the Navier–Stokes equation should be satisfied with simple boundary conditions. We also take $W(\boldsymbol{r})$ to be a real function, for convenience; this means that the axial velocity oscillates with the same (or opposite) phase everywhere, and is equivalent to the condition that the frequency parameter α^2 (equation (1.5)) is small.

The discussion of §2 shows that the secondary flow can influence the solute flux only if W depends on ϕ, because otherwise all fluid particles on a secondary streamline have the same axial velocity. The linearity of (3.8) means that a general ϕ-dependence can be investigated by Fourier analysis, but, again for simplicity, we restrict attention to one Fourier mode, taking

$$W = W_0(r)\cos\phi = \tfrac{1}{2}W_0(\mathrm{e}^{\mathrm{i}\phi} + \mathrm{e}^{-\mathrm{i}\phi}). \tag{3.11}$$

(For consistency with the axial component of the Navier–Stokes equations this requires small axial Reynolds number as well as small α^2; actually to realize such a

velocity field would require a highly artificial distribution of axial body force or pressure gradient, but the idealization makes the mass transfer problem tractable and informative.) A solution is now sought in the form

$$c = C_+(r)\,\mathrm{e}^{\mathrm{i}\phi} + C_-(r)\,\mathrm{e}^{-\mathrm{i}\phi}, \tag{3.12}$$

where $C_\pm$ are complex functions, and (3.8) gives

$$\frac{1}{r}\frac{\mathrm{d}}{\mathrm{d}r}\left(r\frac{\mathrm{d}C_\pm}{\mathrm{d}r}\right) - \left(\frac{1}{r^2} + \mathrm{i}P\omega \pm \mathrm{i}P\frac{V(r)}{r}\right)C_\pm = -\tfrac{1}{2}PW_0(r), \tag{3.13}$$

to be solved subject to the boundary conditions

$$\frac{\mathrm{d}C_\pm}{\mathrm{d}r} = 0 \quad \text{at } r = 1, 1+\delta. \tag{3.14}$$

The final result should be an expression for the excess flux F, which is given by (3.9) to be

$$F = \frac{\pi}{2A}\int_1^{1+\delta} W_0\,\mathrm{Re}\,(C_+ + C_-)\,r\,\mathrm{d}r. \tag{3.15}$$

Because of the functional form (3.10) chosen for V, the solution of (3.13) can be written down in the form of integrals of W_0 multiplied by complex Bessel functions. However, the integrals are difficult to interpret, and it is easier either to solve (3.13) numerically or to simplify further and perform asymptotic expansions in the limits $\delta \ll 1$ and $P \gg 1$. The latter is done in the next section, while the numerical solution of (3.13) is described in §5.

4. Asymptotic expansions

Here we simplify the problem further by assuming a narrow gap ($\delta \ll 1$), so that the dimensionless cross-sectional area $A = 2\pi\delta$, and we concentrate on large secondary-flow Péclet number ($P \gg 1$). We change the radial variable to $x = (r-1)/\delta$, $0 \leqslant x \leqslant 1$, so that, to leading order in δ, (3.13) is

$$\frac{\mathrm{d}^2C_\pm}{\mathrm{d}x^2} - \delta^2[1 + \mathrm{i}P\omega \pm \mathrm{i}PV]C_\pm = -\tfrac{1}{2}\delta^2 PW_0, \tag{4.1}$$

the boundary conditions are

$$\frac{\mathrm{d}C_\pm}{\mathrm{d}x} = 0 \quad \text{at } x = 0, 1$$

and

$$F = \tfrac{1}{4}\mathrm{Re}\,(I_+ + I_-) \quad \text{where } I_\pm = \int_0^1 W_0 C_\pm\,\mathrm{d}x. \tag{4.2}$$

In the limit $\delta \ll 1$, (3.10) requires that $V(x)$ is either linear in x or constant; we assume the same for $W_0(x)$. That is, either there is significant shear in the V- or W_0-profile, or there is not.

Case 1. *No shear* $V = 1$, $W_0 = 1$. Here the only non-uniformity in velocity is the ϕ-dependence of W (equation (3.11)) and the only way solute molecules can be redistributed between fluid particles with different axial velocities is by azimuthal diffusion, represented by the 1 in the square bracket of (4.1). If this were absent, the

solutions for $C_\pm$ would be purely imaginary, so (4.2) gives $F = 0$ as expected. With the 1 present, (4.1) and (4.2) give

$$C_\pm = \frac{P}{2[1+\mathrm{i}P(\omega\pm 1)]}, \quad F = \tfrac{1}{4}P\frac{[1+P^2(1+\omega^2)]}{1+2P^2(1+\omega^2)+P^4(1-\omega^2)^2}. \tag{4.3}$$

Thus
$$F \sim \frac{(1+\omega^2)}{4P(1-\omega^2)^2} \to 0 \tag{4.4}$$

as $P \to \infty$, unless $\omega^2 - 1 = O(P^{-1})$ in which case $F = O(P)$ as $P \to \infty$; if $\omega^2 = 1$, then

$$F \sim \tfrac{1}{8}P \tag{4.5}$$

as $P \to \infty$. Thus even in this simple example there is a *resonance* at $\omega = \pm 1$, when the oscillation period is the same as the time for one secondary-flow circuit, and the flux increases by a factor of $O(P^2)$. Such resonance recurs in the less trivial examples examined below, as discussed in physical terms in §2. We note that if V had been taken equal to zero, the result (4.3) would be

$$F = \frac{P}{4(1+P^2\omega^2)}, \tag{4.6}$$

the result of the Watson theory for this case. Except at resonance, the secondary flow does not affect the large-P scaling of this result, merely modifying the numerical factor multiplying P^{-1}.

Case 2. $V = 1$, $W_0 = x$. Here there is axial shear, so radial diffusion is not negligible, but the lack of secondary shear means that, except at resonance, the result should again exhibit the scaling predicted by Watson's theory. Equation (4.1) can once more be solved exactly, and the solution that satisfies the boundary conditions contains a core term linear in x, which however contributes to the excess flux F only as a result of *azimuthal* diffusion, and terms exponential in x, which represent concentration boundary layers at the walls whose thickness is $O(P^{-\frac{1}{2}})$ as $P \to \infty$. Despite the more complex structure, the excess flux scales approximately as in Case 1; the calculations are straightforward. As $P \to \infty$ with $|\omega^2 - 1| \gg P^{-1}\delta^{-2}$, F is given by (4.4) multiplied by a factor $(\frac{1}{3} + 1/\delta^2)$ of which the larger δ^{-2} term comes from radial diffusion in the boundary layers. As resonance is approached, i.e. as $|\omega^2 - 1|$ approaches zero, F again increases, to a maximum of $\frac{1}{32}P$ when $\omega^2 = 1$, the same order of magnitude as in Case 1.

Case 3. $V = V_0 + x$, $W_0 = x$. In this case there is substantial azimuthal shear, as well as axial shear, and we have introduced a constant V_0 in order to allow the possibility of a line of zero secondary velocity, either in the interior of the annulus or at one of the walls. The governing equation (4.1) becomes

$$\frac{\mathrm{d}^2 C_\pm}{\mathrm{d}x^2} - (\pm \mathrm{i}Q)\left(x - \alpha_\pm \pm \frac{1}{\mathrm{i}P}\right)C_\pm = -\tfrac{1}{2}Qx, \tag{4.7}$$

where $Q = \delta^2 P$ and $\alpha_\pm = -(V_0 \pm \omega)$. The analysis that follows is directed at finding the asymptotic form of the flux function F as $Q \to \infty$; *a fortiori*, $P \to \infty$, and we shall henceforth neglect the term $\pm 1/\mathrm{i}P$, which represents azimuthal diffusion and is never important in this case. As a check for consistency, and also as a demonstration of the essential similarity of this model problem to the more realistic one of unsteady flow in a curved tube at small values of the Dean number (Sharp 1987, see above),

we shall also present, in §5, a numerical solution of (4.7), for values of Q that are not necessarily large.

The substitution

$$C_\pm = \pm\tfrac{1}{2}\mathrm{i}[-1+\alpha_\pm(\pm\mathrm{i}Q)^{\frac{1}{3}}g_\pm(z)], \tag{4.8}$$

where

$$z = (\pm\mathrm{i}Q)^{\frac{1}{3}}(x-\alpha_\pm), \tag{4.9}$$

reduces (4.7) to the inhomogeneous form of Airy's equation; the solution is

$$g_\pm = \mathrm{Fi}_\pm(z)+a_\pm\,\mathrm{Ai}\,(z)+b_\pm\,\mathrm{Bi}\,(z), \tag{4.10}$$

where $a_\pm$, $b_\pm$ are determined from the boundary conditions, Ai, Bi are the standard Airy functions, and

$$\mathrm{Fi}_\pm(z) = \mp\mathrm{i}\int_0^{\infty\mathrm{e}^{\mp\mathrm{i}\pi/6}} \exp[\mp\mathrm{i}(\tfrac{1}{3}t^3+zt)]\,\mathrm{d}t. \tag{4.11}$$

(This is the same as $\pi\,\mathrm{e}^{\mp 2\pi\mathrm{i}/3}\,\mathrm{Hi}\,(z\,\mathrm{e}^{\mp 2\pi\mathrm{i}/3})$ as defined by Olver 1974, pp. 430–432). The asymptotic expansions as $|z|\to\infty$ of the functions appearing in (4.10) and their derivatives will be required; we list them in Appendix A for reference.

The contributions of the three terms in (4.10) to the integrals $I_\pm$ in (4.2) can be computed directly from the asymptotic expansions as long as $|z|$ remains large throughout the range of integration, but that is not the case if $x=\alpha_\pm$ anywhere in that range. Thus for each sign, plus or minus, there are three different cases to consider: (*a*) $\alpha_\pm<0$, (*b*) $\alpha_\pm>1$ and (*c*) $0<\alpha_\pm<1$, with narrow transition regions in between.

(*a*) Here $x-\alpha_\pm>0$ throughout the annulus, so (4.9) gives $z = s\,\mathrm{e}^{\pm\mathrm{i}\pi/6}$, where $s = Q^{\frac{1}{3}}(x-\alpha_\pm)\to+\infty$ as $Q\to\infty$. Of the three terms in (4.10), the second turns out to be exponentially small except in a boundary layer near $x=0$, and the third to be exponentially small except in a boundary layer near $x=1$. The first term in (4.10) is of similar order throughout the annulus, and can be thought of as the 'core' term. Recalling that it is only the real parts of $C_\pm$ that contribute to the flux F through the integrals $I_\pm$ (equation (4.2)), we note that the leading term in the core ($\mathrm{Fi}_\pm\sim -1/z$, equation (A 1)) contributes nothing to the flux. The contributions to $I_\pm$ from the second core term ($-2/z^4$) are

$$\mathrm{Re}\,(I_\pm^{\mathrm{Fi}}) \sim \frac{1-3\alpha_\pm}{6Q(-\alpha_\pm)(1-\alpha_\pm)^3}, \tag{4.12}$$

where $-\alpha_\pm = V_0\pm\omega>0$. The contribution from the $a_\pm$ Ai-term (the boundary layer at $x=0$) turns out to be $O(Q^{-\frac{3}{2}})$ and is therefore negligible compared with (4.12). However, the $b_\pm$ Bi-term (the boundary layer at $x=1$) contributes the following $O(Q^{-1})$ quantity to $I_\pm$:

$$\mathrm{Re}\,(I_\pm^{b}) \sim \frac{-\alpha_\pm}{2Q(1-\alpha_\pm)^3}. \tag{4.13}$$

The difference between the two boundary-layer contributions arises because, in the integral (4.2), $W_0(\equiv x)$ is zero at $x=0$ but not at $x=1$. Combining (4.12) and (4.13) we obtain

$$\mathrm{Re}\,[I_\pm] = \frac{1-3\alpha_\pm+3\alpha_\pm^2}{6Q(-\alpha_\pm)(1-\alpha_\pm)^2}; \tag{4.14}$$

the actual contribution to the excess flux F depends on whether both α_+ and α_- are negative, and the different cases will be examined later.

(*b*) Here $\alpha_\pm>1$, $x-\alpha_\pm<0$ throughout the annulus, so now $s\to-\infty$ as $Q\to\infty$, and the asymptotic expansions (A 3) must be used for the second and third terms in

(4.10). The results, however, are unchanged, and we conclude that $I_\pm$ is given by (4.14) for all $\alpha_\pm$ outside the range $[0, 1]$.

(*c*) $0 < \alpha_\pm < 1$, so $z = 0$ in the interior of the annulus, with the consequence that the asymptotic expansions (A 1–A 3) cannot be used in a neighbourhood of $x = \alpha_\pm$ of thickness $O(Q^{-\frac{1}{3}})$; we call this region the *critical layer*. As long as $\alpha_\pm$ is not within $O(Q^{-\frac{1}{3}})$ of 0 or 1, however, it can be seen that the Ai-, Bi-terms in (4.10) are still exponentially small except in layers at the wall, and that their dominant contribution to $I_\pm$ is $O(Q^{-1})$ and is given by (4.13). Thus we consider only $\mathrm{Fi}_\pm(z)$. If z is written $\mathrm{e}^{\pm \mathrm{i}\pi/6}s$, then, from (4.8), the required integrals (4.2) become

$$I_\pm = \pm\tfrac{1}{2}\mathrm{i}\left[-\tfrac{1}{2}+\alpha_\pm \int_{-\infty}^{\infty} (\alpha_\pm + Q^{-\frac{1}{3}}s)\,\mathrm{Fi}_\pm(\mathrm{e}^{\pm \mathrm{i}\pi/6}s)\,\mathrm{e}^{\pm \mathrm{i}\pi/6}\,\mathrm{d}s\right]. \tag{4.15}$$

From the definition (4.11) of $\mathrm{Fi}_\pm$, it follows that

$$\mathrm{Re}\,(I_\pm) = \tfrac{1}{2}\pi\alpha_\pm^2 \tag{4.16}$$

(see Appendix B), which is $O(1)$ as $Q \to \infty$ and therefore dominates the other contributions.

The above calculations can be combined to give asymptotic expansions for the excess flux F for all values of V_0 and ω except those for which the critical layer is at one of the boundaries, i.e. $\alpha_\pm$ or $(1-\alpha_\pm)$ is $O(Q^{-\frac{1}{3}})$. These cases can be treated analytically, but the transition between cases already analysed is revealed by numerical solution of (4.7) to be smooth and of no great interest, except for the particular case in which α_+ or α_- is close to zero. In this case the critical layer is close to the inner wall of the annulus, $x = 0$, where the axial velocity is zero, and the contribution to the flux is small. In particular, if α_- is exactly zero, the leading contribution (4.15) to $\mathrm{Re}\,(I_-)$ is then identically zero, and the azimuthal diffusion term, $1/\mathrm{i}P$, in (4.7) is required to make $\mathrm{Re}\,(I_-)$ non-zero. A little analysis shows that the dominant term in $\mathrm{Re}\,(I_-)$ is then $O(Q^{-\frac{1}{3}}P^{-1})$, which is negligible compared with $\mathrm{Re}\,(I_+)$, whether that is given by (4.14) or (4.16).

We use the formulae (4.14) and (4.16) to calculate the excess flux F in the limit $Q \to \infty$ for various values of the frequency ω, chosen to be positive without loss of generality. The results of course depend on the value of V_0, representing the secondary velocity at the inner wall of the annulus; results are quoted for all typical cases except those for which the critical layer is at a boundary.

Suppose first that $V_0 > 0$, then α_- is always negative so I_- is given by (4.14). If, in addition, $\omega < V_0$ or $\omega > 1 + V_0$, then α_+ does not lie between 0 and 1, and I_+ is also given by (4.14). Thus the excess flux F (equation (4.2)) is given by

$$F = \frac{1}{24Q}\left(\frac{1+3(V_0+\omega)+3(V_0+\omega)^2}{(V_0+\omega)(1+V_0+\omega)^3} + \frac{1+3(V_0-\omega)+3(V_0-\omega)^2}{(V_0-\omega)(1+V_0-\omega)^3}\right). \tag{4.17}$$

The limits as $\omega \to 0$ and $\omega \to \infty$ are of interest: as $\omega \to 0$,

$$F \sim \frac{1}{12QV_0}\left[1-\left(\frac{V_0}{1+V_0}\right)^3\right]; \tag{4.18}$$

as $\omega \to \infty$,

$$F \sim \frac{1}{4Q\omega^2}. \tag{4.19}$$

If $V_0 < \omega < 1 + V_0$, then there is a critical layer and I_+ is given by (4.16), so that

$$F = \tfrac{1}{8}\pi(V_0-\omega)^2. \tag{4.20}$$

Now suppose that $V_0 < 0$. If $V_0 < -1$, then α_+ is always greater than 1, and the results are very similar to those given above: F is given by (4.17) if ω does not lie between $-(1+V_0)$ and $-V_0$, and is given by

$$F = \tfrac{1}{8}\pi(V_0+\omega)^2 \tag{4.21}$$

if ω does lie in that range. However, if $-1 < V_0 < 0$, it is possible for a critical layer to appear in the solution for both g_+ and g_-. In that case, i.e. $0 \leqslant \omega < \min(1+V_0, -V_0)$, both I_+ and I_- are given by (4.16), so

$$F = \tfrac{1}{4}\pi(V_0^2+\omega^2). \tag{4.22}$$

The above results correspond with the heuristic predictions of the order of magnitude of $\mathscr{D}$ made in §2. We recall that $\mathscr{D} = \omega F/2\pi$, from (3.7); since V_0 and ω are taken to be $O(1)$, we see that (4.20) to (4.22) indeed give $\mathscr{D} \sim 1$, as predicted for the case of resonance with secondary shear at the end of §2. Moreover, in the limit $\omega \to \infty$ (i.e. $t_s \gg T$) one would expect the secondary motion to become unimportant, so that result should reduce to Watson's (1983) predictions for straight-tube flow; equation (4.19) is indeed the result obtained from that theory for axial Couette flow in an annulus with velocity amplitude $w_0/\sqrt{2}$ at $x = 1$ (equal to the azimuthal r.m.s. axial velocity amplitude in our case):

$$\mathscr{D} = \frac{1}{8\pi\delta^2 P\omega} = \frac{\kappa}{8\pi\delta^2 a^2\hat{\omega}} \sim \frac{T}{t_d}$$

(cf. (2.7)).

5. Numerical solutions

5.1. *Confirmation of asymptotics for Case* 3

We have also solved (4.7) numerically, retaining the term $(\pm 1/\mathrm{i}P)$ representing diffusion in the azimuthal (ϕ) direction. Thus, in contrast to the asymptotic analysis, the numerical results are valid for arbitrary Q and P.

A solution to (4.7), with the zero-flux condition imposed at the walls, was obtained using a finite-difference method accurate to second order. The resulting complex coefficient matrix constituted a tridiagonal system that was solving using L–U decomposition and a subsequent back substitution to solve for $C_\pm(x)$. The dimensionless flux F and axial diffusivity $\mathscr{D}$ were then calculated by use of (3.15) and (3.7), respectively.

The distribution of $\mathrm{Re}\{W_0(x)[C_+(x)+C_-(x)]\}$ is useful as a *local* measure of axial transport. With regard to our earlier discussion (§2), the zone in which this quantity is largest delineates the effective transport area represented by $\mathscr{A}$. For the results shown in figure 4, $\omega = 1.5$, $V_0 = 1$, and $\delta = 0.1$; hence the critical layer is centred about $x = 0.5$. The three curves shown for $Q = 10^2$, 10^3 and 10^4 are consistent with the scaling predictions $\delta_c \propto Q^{-\frac{1}{3}}$ of §§2 and 4.

Figure 5 shows the distribution of $\mathrm{Re}\{W_0(x)[C_+(x)+C_-(x)]\}$ for $\omega = 10$ and $Q = 10$, 10^2 and 10^3, demonstrating the dominant influence on transport exerted by the boundary layer of thickness $(P\omega)^{-\frac{1}{2}}$ on the wall $x = 1$. For $\omega < 1$ (figure 6) the contribution to F is somewhat more uniformly distributed over the annulus. In both figures the contribution to the flux is negative in the core and positive in the boundary layer on $x = 1$, as can be deduced from (4.12) and (4.13).

By choosing a value for $Q \gg 1$, a direct quantitative comparison can be made between the asymptotic theory and the numerical prediction. In figure 7 we plot the

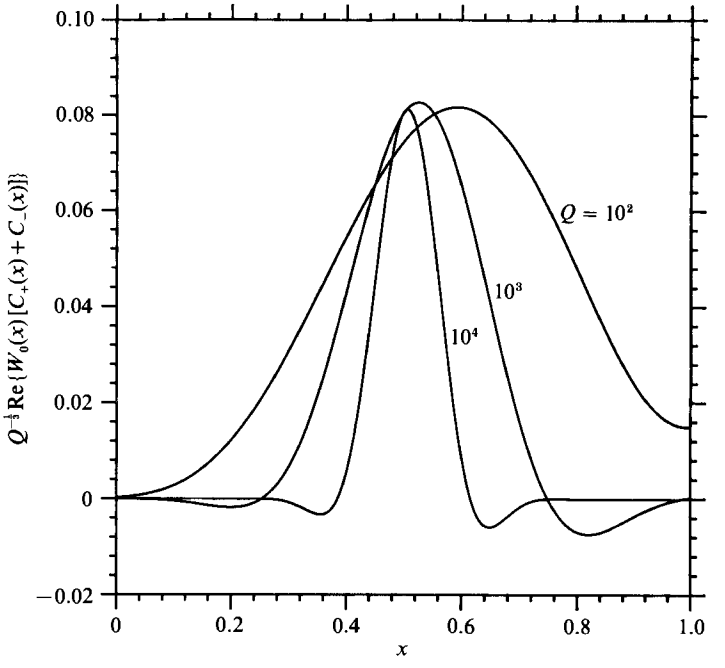

FIGURE 4. Distribution of $Q^{-\frac{1}{3}}\,\mathrm{Re}\{W_0(x)[C_+(x)+C_-(x)]\}$ across the annulus for $\omega = 1.5$, $V_0 = 1$, $\delta = 0.1$, $Q = \delta^2 P = 10^2$, 10^3, and 10^4.

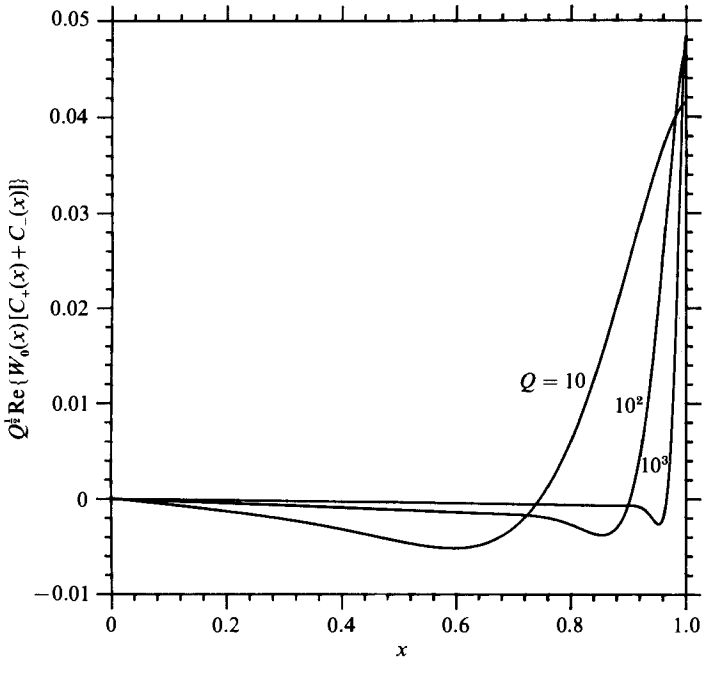

FIGURE 5. Distribution of $Q^{\frac{1}{2}}\,\mathrm{Re}\{W_0(x)[C_+(x)+C_-(x)]\}$ across the annulus for $V_0 = 1$, $\delta = 0.1$, $\omega = 10$, $Q = 10$, 10^2, and 10^3.

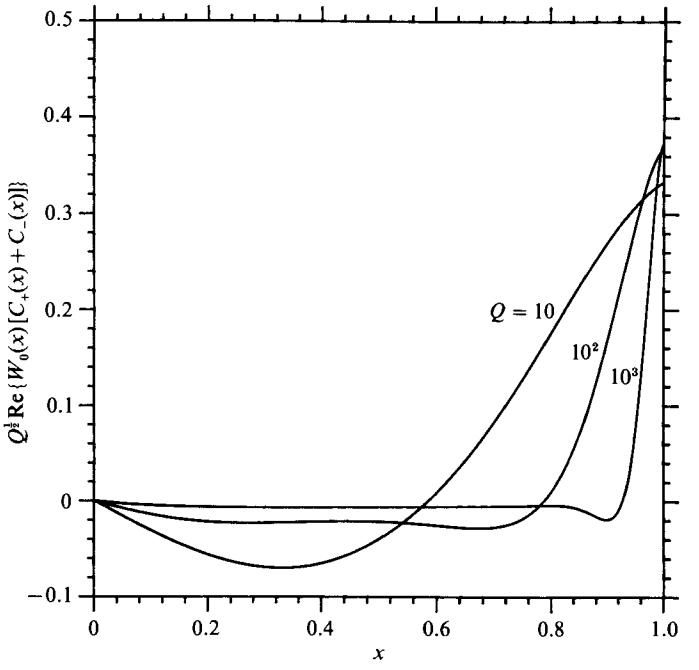

FIGURE 6. Distribution of $Q^{\frac{1}{2}}\,\mathrm{Re}\{W_0(x)[C_+(x)+C_-(x)]\}$ across the annulus for $V_0 = 1$, $\delta = 0.1$, $\omega = 0.1$, $Q = 10$, 10^2, and 10^3.

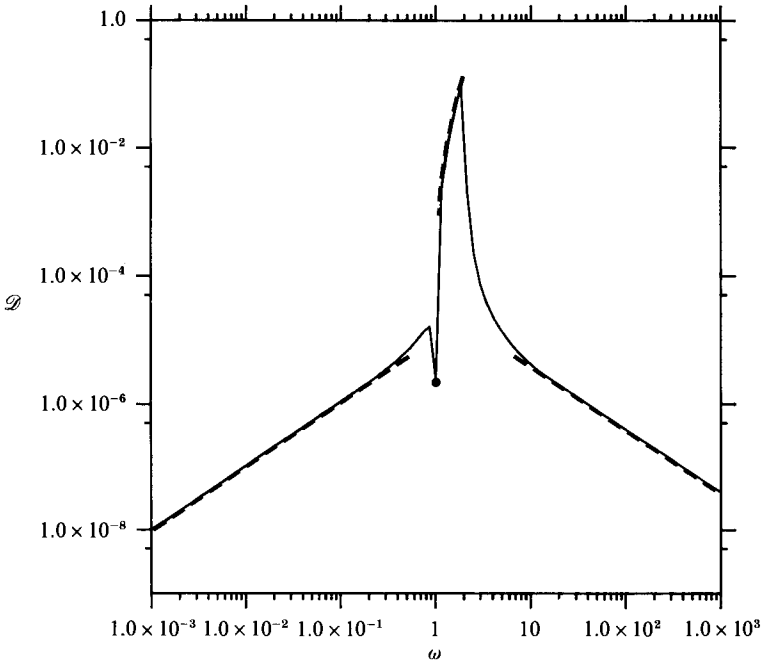

FIGURE 7. Normalized diffusivity $\mathscr{D}$ for a narrow annulus plotted against ω for $V_0 = 1$, $Q = 10^3$. Solid line: numerical solution with $\delta = 0.1$. Dashed line: asymptotic solutions for $Q \to \infty$ and $\omega \to 0$ (equation (4.18)); $\omega \to \infty$, (4.19); and $V_0 < \omega < (1 + V_0)$, (4.20). The point at $\omega = 1$ is also obtained from the analysis.

numerical results for $Q = 10^3$ in terms of the transport parameter $\mathscr{D}$. Also shown are the predictions of the asymptotic theory for the three cases of §4, Case 3: (i) $\omega \to 0$, (equation (4.8)), (ii), $\omega \to \infty$, (4.19) and (iii) $V_0 < \omega < (1+V_0)$, (4.20). Moreover the dip in the curve at $\omega = 1$ can also be explained by the asymptotic theory; $\alpha_- = 0$ at that value of ω so I_- does not contribute to the flux, and $\alpha_+ = -2$ so $\mathrm{Re}\,(I_+) = 19/324Q$, from (4.14), and $F = \frac{1}{4}\,\mathrm{Re}\,(I_+)$. The corresponding point is marked on figure 7. In all cases the agreement is excellent, confirming the validity of both the asymptotic results (for $Q \gg 1$) and the numerical scheme.

5.2. *Computations for a wide annulus*

With the aim of producing a model that more closely mimics the process of axial dispersion in a curved tube, we now examine transport in a wide annulus; $\delta \sim O(1)$. The narrow-gap approximation leading to (4.7) is therefore no longer valid and we solve instead (3.13) with boundary conditions (3.14). As before, the full equation (including circumferential diffusion) is solved numerically by a second-order finite-difference scheme.

For the numerical example considered here, $\delta = 1$, $Q = P$, $V(r) = 2/r$ and $W_0(r) = r - 1$. Since we normalize radial distance by the inner radius of the annulus, the axial velocity varies between zero and one across the annulus, as in §4. The profile chosen for $V(r)$ is a typical member of the family given by (3.10) that incorporates shear in the secondary flow (i.e. is not solid-body rotation).

Computed values for $\mathscr{D}$ as functions of $\beta^2 (= t_d/T)$ are shown in figure 8 for values that are both large and small compared with one. Clearly visible for large P is the peak in $\mathscr{D}$, of $O(1)$, corresponding to the resonance condition (for the case chosen here, resonance occurs if $0.5 < \omega < 2.0$), and therefore occurring at values of β^2 roughly proportional to P since $\omega \propto \beta^2/P$. As P is reduced the peak becomes less pronounced, and it is frozen at a fixed value of $\beta^2 (\approx 1)$ for small $P (\leqslant 10^{-1})$ when the effects of secondary flow are negligible. At sufficiently high ω, all results approach a single curve of the form $\mathscr{D} \propto \beta^{-2}$, whereas for $\omega < 1$, $\mathscr{D} \propto \beta^2 P^{-2}$ for $P \geqslant 10$. Both results are consistent with the analytical predictions of §4. When $P \leqslant 10^{-1}$ and $\omega < 1$, $\mathscr{D} \propto \beta^2$, consistent with the quasi-steady result in the absence of secondary flow.

These same results are plotted on a contour map in figure 9, showing more clearly the different types of behaviour. The ridge running diagonally across the figure corresponds to the condition $\omega \sim 1$. Another ridge of maximal $\mathscr{D}$ is located along $\beta^2 \approx 1$ for $\omega < 1$.

This complex pattern of behaviour can be explained using the heuristic arguments of §2, for the separate zones indicated in the figure. In Zone 1 ($\beta^2 < 1, P < 1$) both T and t_s are large compared with the diffusive time. Consequently, the result is as predicted for quasi-steady transport in a 'quasi-straight' tube (i.e. one in which secondary motions are unimportant): $t_c \sim t_d$ and $w_{rel} \sim w_0$, leading to $\mathscr{D} \propto \beta^2$.

As oscillation frequency increases, we enter zone 2 which, for $P < 1$, is simply the high-frequency, straight-tube result. As the results show, however, this behaviour persists for $P > 1$ up to $\omega \approx 1$. In this latter region, although $t_s < t_d$, T is smaller still; the axial velocity will be correlated over either T or t_s owing to migration in the shear flow by molecular diffusion. The shorter uncorrelation time, T in this case, is appropriate to use in (2.4), giving the observed result, $\mathscr{D} \propto \beta^{-2}$.

Zone 3 is entered from Zone 1 by increasing P, thereby introducing the effects of secondary flow. The change in behaviour found on entering Zone 3 is, in a sense, analogous to that experienced in passing from Zone 1 into Zone 2. The analogy

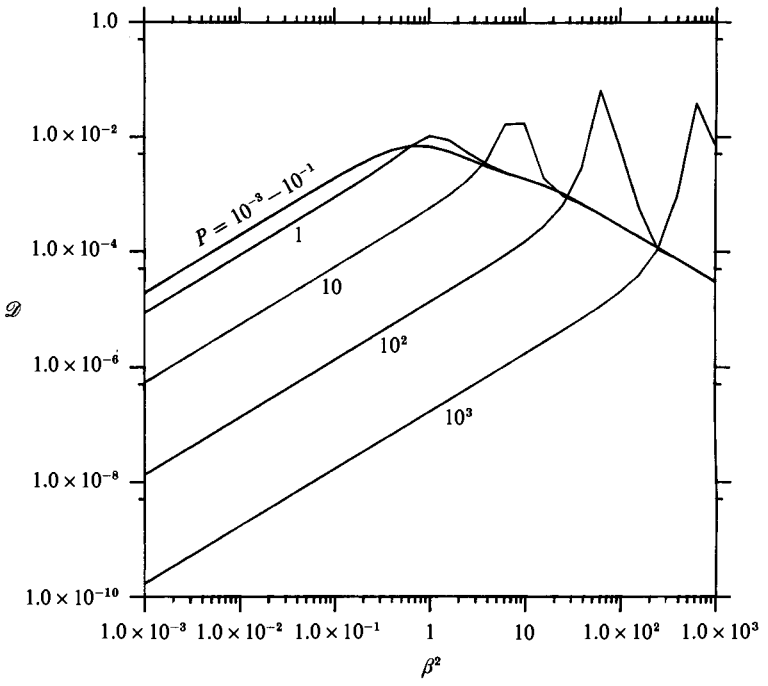

FIGURE 8. Numerical solution of normalized diffusivity $\mathscr{D}$ for a wide annulus ($\delta = 1.0$) plotted against β^2 for $10^{-3} < Q < 10^3$. Variations near the peaks are only coarsely resolved owing to the limited number of numerical points.

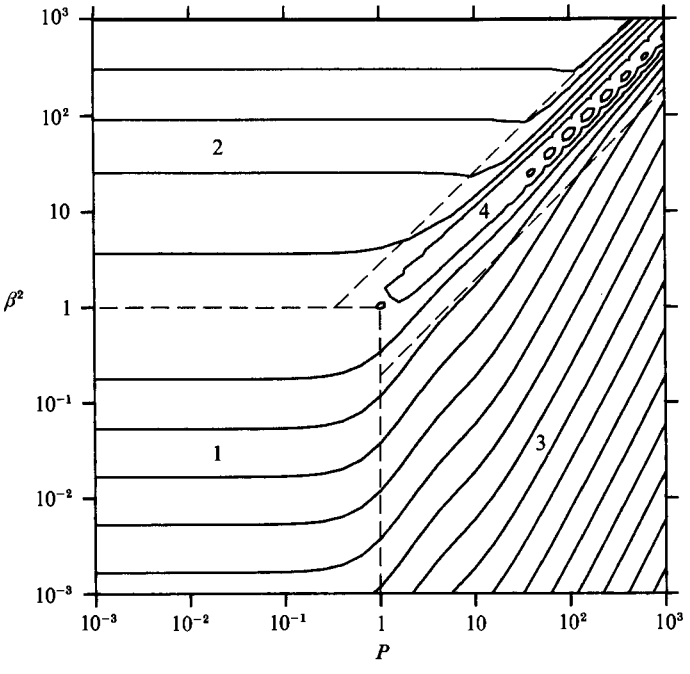

FIGURE 9. Contour plots of the results shown in figure 8 showing $\mathscr{D}$ mapped onto the (β^2, P)-plane. Dashed lines delineate the different zones discussed in the text.

follows from the observation that, as a fluid particle is advected around the annulus, its axial velocity oscillates owing to the ϕ-dependence of W, just as, in the absence of secondary motion, it oscillates owing to time-periodic motion at a fixed location. As a particle traverses a secondary flow circuit, it can travel either faster or slower than the mean owing to diffusion in the shear field. Consequently, the particle experience a relative velocity proportional to the product of the diffusion distance in time t_s, $(\kappa t_s)^{\frac{1}{2}}$, and the velocity gradient (w_0/a). The persistence time is t_s, giving the result from (2.4), $\mathscr{D} \propto P^{-2}\beta^2$. The analogy between Zones 2 and 3 is more evident if we use t_s in the normalization of D_{eff}, giving $D_{\text{eff}}/(w_0^2 t_s) = P^{-1}$. This behaviour, we note, is distinctly different from that observed during quasi-steady flow in a curved tube, for the reasons discussed in §2.

The arguments leading to a prediction for Zone 4 are found in §2. Here we merely note that the previous prediction, that $\mathscr{D} \propto O(1)$, is supported by the numerical result.

6. Discussion

The objective of this study was to gain new insights into the mechanism of axial transport in unsteady tube flows influenced by secondary motions. It is therefore appropriate to ask to what extent our model problem can be generalized to flows of greater practical importance. As discussed in §1, the most direct analogue is oscillatory flow in a curved tube, for which some preliminary numerical results were presented in figure 1. There are indeed strong similarities between these results and the model predictions, as can be seen by comparing figure 1 with the contour plot of the model calculation (figure 9). The regions indicated in figure 9 as Zones 1 and 2, exhibiting the character of a 'quasi-straight' tube, are also seen in figure 1. So is the ridge associated with a maximum in transport rate [$\mathscr{D} \sim O(1)$] at $\omega \approx 1$ (Zone 4). The model thus supports our earlier claim that the peak in transport rate is associated with a condition of resonance, producing a rectified axial particle displacement through an interaction between the time-periodic axial flow and the secondary circulation.

Some differences are evident, however, in Zone 3 ($\omega > 1$). In the curved tube, $\mathscr{D}$ becomes independent of P ($= Dn^2Sc$) as $P \to \infty$ (and hence $\omega \to 0$, for fixed t_d/T), whereas the model prediction continues to fall, in proportion to ω/P (from (4.18) and (3.7)). In both cases the initial fall in $\mathscr{D}$ as P increases results from a progressive enhancement of cross-sectional mixing due to the secondary flow. However, in the limit of perfect mixing along the secondary-flow streamlines, the average axial velocities of all particles on a particular secondary streamline are the same, zero for every streamline in our model problem because $W \propto \cos\phi$. Since in the model this velocity is the same for all streamlines then, in the limit of perfect mixing along a streamline, all fluid travels at the same average speed and $\mathscr{D} \to 0$. In the curved tube, on the other hand, $\mathscr{D}$ asymptotically approaches a non-zero limit. This difference can be attributed to the non-uniform distribution of axial particle velocities that persists in a curved tube even when perfect mixing along secondary streamlines is achieved.

This result is easily demonstrated mathematically. If, in the model, we let $W = W_0(r)(1+\cos\phi)$, then the average velocity along a streamline is $W_0(r)$ rather than zero. Concentration can be represented by $C = C_+ e^{i\phi} + C_- e^{-i\phi} + C_0$ where the new term, C_0, satisfies

$$i\omega C_0 = W_0(r) + \frac{1}{r}\frac{d}{dr}\left\{r\frac{dC_0}{dr}\right\}.$$

This is the same governing equation as obtains in the absence of secondary flows (cf. Watson 1983) and leads to an additive contribution to the flux and to the axial diffusivity. This contribution is negligible over much of the parameter space but is evident in the low-ω, high-P regime of figure 1.

The most striking feature exhibited by the model is the critical layer associated with the condition of 'resonance' between the oscillation period and the circulation time. To the extent that resonance may be expected to occur more generally, it provides a potentially important means of enhancing the rate of axial transport in many applications. Resonance occurs when, in the absence of molecular diffusion, a fluid particle exhibits a net displacement from its initial position that is linear in time rather than periodic. Viewed in this way, the existence of a critical layer can be identified by determining conditions for which the Lagrangian axial displacement of a particle, $z(t)$, becomes unbounded at $t \to \infty$.

In an oscillatory flow of fundamental frequency Ω and with fixed, closed secondary streamlines, the secondary flow, like the axial, will be unsteady and dependent on position on the streamline. On a given streamline the secondary velocity of a particle will consist of a mean value V_s together with oscillations at frequencies that are multiples of the rotation frequency V_s/P, where P is the streamline perimeter. It follows that a particle's axial velocity will contain these frequencies as well as multiples of the oscillation frequency Ω, coupled in a nonlinear way that gives a non-zero mean value for a number of different values of Ω. Thus there may be several possible resonant frequencies for each streamline. Moreover, since the rotation frequency will in general vary between streamlines (in the case of flow in a curved tube it takes all values between zero and infinity) there may well be several streamlines on which resonance occurs for any given frequency, leading to the intriguing possibility of a large number of critical layers.

Another potentially important effect in practical flows is associated with periodic *variations* in the secondary-streamline pattern. In a curved tube, for example, these occur if either the secondary flow is not quasi-steady ($\alpha^2 > 1$; see Lyne 1971) or the maximum value of the Dean number is large (or both). This could, in effect, produce efficient transverse mixing over the tube cross-section on the convective timescale t_s rather than the diffusive timescale t_d. The result would be a smearing of the resonant peak and a consequent reduction in the contribution to $\mathscr{D}$ from the neighbourhood of $\omega \sim 1$; this may be the explanation for the downward slope of the diagonal ridge in figure 1. In addition, greater cross-sectional mixing would decrease $\mathscr{D}$ in Zone 1 (quasi-steady and quasi-straight), but increase it in Zones 2 and 3 in that a fluid particle would sample a wide range of axial velocities during the persistence time of T or t_s, in Zones 2 and 3 respectively.

As a final point, one might ask what these results tell us about gas transport during high-frequency pulmonary ventilation (HFV), which provided the original motivation for this study. The geometrical complexity of the lung means that the idealizations made here can be expected to give no more than a rough qualitative indication of pulmonary transport (for example, the absence of fully developed flow means that the concept of effective diffusivity is itself a crude approximation). Nevertheless, we can see that when the secondary motions exhibit ordered structures, as has been observed in model bifurcations (Schroter & Sudlow 1969), the effect on transport may be very different from what one would predict based on an assumption of turbulent-like mixing. Specifically, there exists the potential for 'tuning' the oscillation frequency so that resonance is achieved, in a particular region of the lung, thereby greatly enhancing the local gas transport rates. Under resonant

conditions, a form of 'streaming' occurs which is distinct from the types of streaming discussed by previous authors. The potential for this form of enhancement is found whenever $t_d/T > 1$ and $P > 1$ and is therefore most likely to be important in the central airways. To appreciate fully what impact this might have on HFV, we need to examine cases in which some convective mixing between streamlines is allowed. This may be the most important factor limiting the amount of transport enhancement possible, and is certain to occur in the lung.

We are grateful to C. G. Phillips for deriving the proof given in Appendix B, and to K. Sharp for providing us with his preliminary numerical results, presented in figure 1. We also gratefully acknowledge the financial support of the US National Science Foundation (Grant no. 8313017-MEA) and the UK Science and Engineering Research Council (Grant no. GR/D/76639).

Appendix A. Asymptotic expansion of the Airy functions appearing in (4.10)

For $z = s\,e^{\pm i\pi/6}$, s (real) $\to \infty$, these can be deduced from Olver (1974), and are as follows:

$$s \to \pm\infty \quad \mathrm{Fi}_\pm(z) \sim -\frac{1}{z} - \frac{2}{z^4}\ldots, \quad \mathrm{Fi}'_\pm(z) \sim \frac{1}{z^2} + \frac{8}{z^5} + \ldots; \tag{A 1}$$

$$s \to +\infty \begin{cases} \mathrm{Ai}(z) \sim \dfrac{1}{2\pi^{\frac{1}{2}}} z^{-\frac{1}{4}} e^{-\zeta}, & \mathrm{Ai}'(z) \sim \dfrac{-1}{2\pi^{\frac{1}{2}}} z^{\frac{1}{4}} e^{-\zeta} \\ \mathrm{Bi}(z) \sim \dfrac{1}{\pi^{\frac{1}{2}}} z^{-\frac{1}{4}} e^{\zeta}, & \mathrm{Bi}'(z) \sim \dfrac{1}{\pi^{\frac{1}{2}}} z^{\frac{1}{4}} e^{\zeta} \end{cases}, \tag{A 2}$$

where $$\zeta = \tfrac{2}{3} z^{\frac{3}{2}};$$

$$s \to -\infty \begin{cases} \mathrm{Ai}(z) \sim \dfrac{1}{\pi^{\frac{1}{2}}} (-z)^{-\frac{1}{4}} \sin(\bar{\zeta} + \tfrac{1}{4}\pi), & \mathrm{Ai}'(z) \sim \dfrac{-1}{\pi^{\frac{1}{2}}} (-z)^{\frac{1}{4}} \cos(\bar{\zeta} + \tfrac{1}{4}\pi) \\ \mathrm{Bi}(z) \sim \dfrac{1}{\pi^{\frac{1}{2}}} (z)^{-\frac{1}{4}} \cos(\bar{\zeta} + \tfrac{1}{4}\pi), & \mathrm{Bi}'(z) \sim \dfrac{1}{\pi^{\frac{1}{2}}} (-z)^{\frac{1}{4}} \sin(\bar{\zeta} + \tfrac{1}{4}\pi) \end{cases}, \tag{A 3}$$

where $$\bar{\zeta} = \tfrac{2}{3}(-z)^{\frac{3}{2}}.$$

Appendix B. Evaluation of added-flux integrals across the critical layer

We seek the real parts of the quantities $I_\pm$ defined in (4.15); i.e. we seek the real parts of

$$I_\pm^{(0)} = \tfrac{1}{2} e^{\pm i\pi/2} \alpha_\pm^2 \int_{-\infty}^{\infty} \mathrm{Fi}_\pm(e^{\pm i\pi/6} s)\, e^{\pm i\pi/6}\, ds,$$

and

$$I_\pm^{(1)} = \tfrac{1}{2} e^{\pm i\pi/2} \alpha_\pm \int_{-\infty}^{\infty} \mathrm{Fi}_\pm(e^{\pm i\pi/6} s)\, e^{\pm i\pi/6} s\, ds.$$

Substituting $t = e^{\pm i\pi/6} u$ in (4.11) gives

$$\mathrm{Fi}_\pm(e^{\pm i\pi/6} s) = e^{\mp i2\pi/3} \int_0^{\infty} e^{-u^3/3}\, e^{\mp isu}\, du.$$

Hence, for $k = 0, 1$,

$$I_{\pm}^{(k)} = \tfrac{1}{4}\alpha_{\pm}^{2-k} \int_{-\infty}^{\infty} \left\{ \int_{-\infty}^{\infty} \mathrm{e}^{-|u|^3/3}\, \mathrm{e}^{-\mathrm{i}su}\, \mathrm{d}u \right\} s^k\, \mathrm{d}s. \tag{B 1}$$

Now, if we let $$f(u) = \mathrm{e}^{-|u|^3/3},$$

the curly bracket in (B 1) is the Fourier transform of f, so f can also be written

$$f(u') = \frac{1}{2\pi} \int_{-\infty}^{\infty} \left(\int_{-\infty}^{\infty} \mathrm{e}^{-|u|^3/3}\, \mathrm{e}^{-\mathrm{i}su}\, \mathrm{d}u \right) \mathrm{e}^{\mathrm{i}su'}\, \mathrm{d}s.$$

Hence $$I_{\pm}^{(0)} = \tfrac{1}{2}\pi\alpha_{\pm}^2 f(0) = \tfrac{1}{2}\pi\alpha_{\pm}^2$$

and $$I_{\pm}^{(1)} = \mathrm{i}\tfrac{1}{2}\pi\alpha_{\pm}^2 f'(0) = 0,$$

from which (4.16) follows.

REFERENCES

Chatwin, P. C. 1975 On the longitudinal dispersion of passive contaminant in oscillatory flows in tubes. *J. Fluid Mech.* **71**, 513–527.

Dean, W. R. 1928 The streamline motion of fluid in a curved pipe. *Phil. Mag.* S7 **5**, 673–695.

Drazen, J. H., Kamm, R. D. & Slutsky, A. S. 1984 High frequency ventilation. *Physiol. Rev.* **64**, 505–543.

Erdogan, E. & Chatwin, P. C. 1967 The effects of curvature and buoyancy on the laminar dispersion of solute in a horizontal tube. *J. Fluid Mech.* **29**, 465–484.

Janssen, L. A. M. 1976 Axial dispersion in laminar flow through coiled tubes. *Chem. Engng Sci.* **31**, 215–218.

Johnson, M. & Kamm, R. D. 1986 Numerical studies of steady flow dispersion at low Dean number in a gently curving tube. *J. Fluid Mech.* **172**, 329–345.

Joshi, C. H., Kamm, R. D., Drazen, J. M. & Slutsky, A. S. 1983 An experimental study of gas exchange in laminar oscillatory flow. *J. Fluid Mech.* **133**, 245–254.

Lévêque, M. A. 1928 Transmission de chaleur par convection. *Ann. Mines* **13**, 201–362.

Lyne, W. H. 1971 Unsteady viscous flow in a curved pipe. *J. Fluid Mech.* **45**, 13–31.

Nunge, R. L., Lin, T.-S. & Gill, W. N. 1972 Laminar dispersion in curved tubes and channels. *J. Fluid Mech.* **51**, 363–383.

Olver, F. W. J. 1974 *Asymptotics and Special Functions.* Academic.

Rhines, P. B. & Young, W. R. 1983 How rapidly is a passive scalar mixed within closed streamlines? *J. Fluid Mech.* **133**, 133–145.

Schroter, R. C. & Sudlow, M. F. 1969 Flow patterns in models of the human bronchial airways. *Respir. Physiol.* **7**, 341–355.

Sharp, K. 1987 Dispersion in a curved tube during oscillatory flow. Ph.D. dissertation, M.I.T.

Taylor, G. I. 1921 Diffusion by continuous movements. *Proc. Lond. Math. Soc.* 2 **20**, 196–212.

Taylor, G. I. 1953 Dispersion of soluble matter in solvent flowing slowly through a tube. *Proc. R. Soc. Lond.* A **219**, 186–203.

Watson, E. J. 1983 Diffusion in oscillatory pipe flow. *J. Fluid Mech.* **133**, 233–244.